

Polarization-resolved Raman spectra of α -PtO_2

Zhanhong Lei(雷展宏), Weiliang Wang(王伟良), and Juncong She(佘峻聪)
Citation: Chin. Phys. B, 2021, 30 (**4**): 047102. DOI: 10.1088/1674-1056/abccb5
Journal homepage: http://cpb.iphy.ac.cn; http://iopscience.iop.org/cpb

What follows is a list of articles you may be interested in

Interfacial properties of g-C_3N_4/TiO_2 heterostructures studied by DFT calculations

Chen-Shan Peng(彭春山), Yong-Dong Zhou(周永东), Sui-Shuan Zhang(张虽栓), and Zong-Yan Zhao(赵宗彦)
Chin. Phys. B, 2021, 30 (**1**): 017101. DOI: 10.1088/1674-1056/abb30b

Vanadium based XVO_3 (X=Na, K, Rb) as promising thermoelectric materials: First-principle DFT calculations

N A Noor, Nosheen Mushahid, Aslam Khan, Nessrin A. Kattan, Asif Mahmood, Shahid M. Ramay
Chin. Phys. B, 2020, 29 (**9**): 097101. DOI: 10.1088/1674-1056/ab99ad

Structural evolution and magnetic properties of $ScLi_n$ (n=2-13) clusters: A PSO and DFT investigation

Lu Li(栗潞), Xiu-Hua Cui(崔秀花), Hai-Bin Cao(曹海宾), Yi Jiang(姜轶), Hai-Ming Duan(段海明), Qun Jing(井群), Jing Liu(刘静), Qian Wang(王倩)
Chin. Phys. B, 2020, 29 (**7**): 077101. DOI: 10.1088/1674-1056/ab8d9e

Ab initio study of structural, electronic, thermo-elastic and optical properties of Pt_3Zr intermetallic compound

Wahiba Metiri, Khaled Cheikh
Chin. Phys. B, 2020, 29 (**4**): 047101. DOI: 10.1088/1674-1056/ab7223

A simple rule for finding Dirac cones in bilayered perovskites

Xuejiao Chen(陈雪娇), Lei Liu(刘雷), Dezhen Shen(申德振)
Chin. Phys. B, 2019, 28 (**7**): 077106. DOI: 10.1088/1674-1056/28/7/077106

Polarization-resolved Raman spectra of α-PtO_2*

Zhanhong Lei(雷展宏)[1], Weiliang Wang(王伟良)[1,†], and Juncong She(佘峻聪)[2]

[1] State Key Laboratory of Optoelectronic Materials and Technologies, Guangdong Province Key Laboratory of Display Material and Technology, School of Physics, Sun Yat-sen University, Guangzhou 510275, China

[2] State Key Laboratory of Optoelectronic Materials and Technologies, Guangdong Province Key Laboratory of Display Material and Technology, School of Electronics and Information Technology, Sun Yat-sen University, Guangzhou 510275, China

(Received 12 October 2020; revised manuscript received 10 November 2020; accepted manuscript online 23 November 2020)

Using density functional theory, we investigate the vibrational properties and polarization-resolved Raman spectra of α-PtO_2 and obtain the Raman tensor and angle-dependent Raman intensity of α-PtO_2. It is found that the polar plot of A_{1g} mode in parallel polarization configuration is useful in identifying the orientation of the crystal. The Raman intensity of the E_g mode is about five times stronger than that of the A_{1g} mode. The Raman intensity is about three times stronger when the wave vector of the incident light is in x or y direction than in z direction. Our work will help the material scientists to characterize the α-PtO_2 and to identify its orientation by comparing the experimental spectra with our result.

Keywords: Raman tensor, DFT, α-PtO_2

PACS: 31.15.E–, 78.30.–j **DOI:** 10.1088/1674-1056/abccb5

1. Introduction

In recent years, the versatility of platinum oxides has attracted extensive attention in different fields. Known as Adams' catalyst, platinum oxides play an important role in industry.[1,2] Abundant researches on the catalytic behavior of platinum oxides have been conducted, such as the oxidation of ammonia,[3] CO oxidation,[4] hydrosilylation reaction[5] and oxidation of ethanol to acetic acid.[6,7] In electrochemistry, the oxidation on the surface of platinum electrodes remarkably influence the reaction processes.[8,9] In electronics, platinum oxides find applications for memory capacitors as electrode materials,[10] as well as nanoscale and molecular electronics.[11]

Five platinum oxide phases have been identified clearly: PtO, Pt_3O_4, α-PtO_2 (hexagonal), β-PtO_2 (orthorhombic), and β'-PtO_2 (tetragonal rutile-type structure).[12,13] Among these phases, α-PtO_2 has raised our attention on account of its promising applications on catalysis as nanoparticles[6] and on nanotechnology as nanotubes.[13] There is theoretical investigation of α-PtO_2 focused on the formation energy,[14] while the vibrational properties and theoretical Raman spectra cannot be found in literature.

Compared with conventional evaporation or sputtering methods of producing α-PtO_2, new approaches such as oxygen plasma treatment to produce ultra-thin platinum-oxide films[11] and hydrolytic reaction to synthesize α-PtO_2 nanocrystals[15] have greatly improved the material's performance and facilitated their applications. However, there exists a problem that α-PtO_2 needs to be characterized from the experimental product PtO_x, where $1 < x < 2.1$ varies under different conditions.[16,17] Different analytic techniques have been applied to confirm existence of α-PtO_2, such as x-ray powder diffraction, scanning electron microscopy and x-ray photoelectron spectra. The Raman spectroscopy, a powerful method to characterize materials with the advantage of identifying the orientation of a crystal,[18,19] has also been applied to investigation of α-PtO_2,[20] but in lack of the corresponding theoretical calculation of Raman spectra. In this work, we calculate the phonon dispersion and polarization-resolved Raman spectra of α-PtO_2 under the frame of density functional theory. We believe that our work will be supplement to previous theoretical researches and will help experimentalists to characterize the α-PtO_2 and to identify its orientation.

2. Calculation method

The structural optimization and calculation of dielectric tensor was performed using the Vienna *ab initio* simulation package within the framework of density functional theory.[21] The exchange-correlation potential was described by generalized gradient approximation using Perdew–Burke–Ernzerhof type functional.[22] The projected augmented-wave method was used to construct plane-wave basis set, and the energy cutoff is 400 eV for structural optimization and 500 eV for force constant calculation.[23] Brillouin zone was sampled on a Γ centered grid of $4 \times 4 \times 4$ k-mesh for structural optimization and force constant calculation and a Γ centered $40 \times 40 \times 40$ k-mesh for dielectric tensor calculation. The convergence of the total energy was set to 10^{-8} eV. The phonon dispersion of

*Project supported by the Key-Area Research and Development Program of GuangDong Province, China (Grant No. 2019B030330001), the National Key R&D Program of China (Grant No. 2016YFA0202000), the Natural Science Foundation of Guangdong Province, China (Grant No. 2018B030311045), the National Natural Science Foundation of China (Grant No. 11704419), and the Physical Research Platform (PRP) in School of Physics, SYSU.

†Corresponding author. E-mail: wangwl2@mail.sysu.edu.cn

© 2021 Chinese Physical Society and IOP Publishing Ltd

α-PtO_2 was calculated using the density functional perturbation theory and Phonopy code for a $3\times3\times3$ supercell.[24]

The Raman intensity of the j-th mode can be obtained by[25]

$$\frac{\mathrm{d}\sigma}{\mathrm{d}\Omega} = N_{\mathrm{prim}}\frac{\omega_s^4}{c^4 V_{\mathrm{prim}}}\left|\boldsymbol{e}_s\cdot\tilde{R}(j)\cdot\boldsymbol{e}_i^{\mathrm{T}}\right|^2\times\frac{\hbar}{2\omega_j}(n_j+1),$$

where ω_i, ω_s and ω_j are the frequencies of incident light, scattered light and the j-th phonon mode respectively; n_j is the Bose factor of the j-th phonon; $\boldsymbol{e}_i(\boldsymbol{e}_j)$ is electric polarization vector of incident (scattered) light. The Raman tensor can be calculated with a finite displacement method[26–38]

$$\tilde{R}_{\alpha\beta}(j) = V_{\mathrm{prim}}\sum_{\mu=1}^{N}\sum_{l=1}^{3}\frac{\partial\chi_{\alpha\beta}}{\partial r_l(\mu)}\frac{e_l^j(\mu)}{\sqrt{M_\mu}},$$

where $\partial\chi_{\alpha\beta}/\partial r_l(\mu)$ is the first derivative of the polarizability tensor computed by moving the atoms along $e_l^j(\mu)/\sqrt{M_\mu}$, $e_l^j(\mu)$ the eigenvectors of j-th phonon mode at Γ point, and M_μ is the atomic mass of atom μ.

3. Results and discussion

The crystal structure of α-PtO_2 is composed of stacked O–Pt–O trilayers, with 3 atoms in each unit cell (Fig. 1). The lattice constants are found to be $a=b=3.164$ Å, $c=4.728$ Å, which are larger than the XRD results $a=b=3.113$ Å, $c=4.342$ Å.[20] There are nine phonon modes in the phonon dispersion of α-PtO_2 (Fig. 2), including six optical modes and three acoustic modes. The six optical modes are A_{1g}, $2E_g$, $2E_u$ and A_{2u}. The two oxygen atoms vibrate relatively in z, y and x directions in A_{1g} (Fig. 3(a)), $E_{g,1}$ (Fig. 3(b)) and $E_{g,2}$ (Fig. 3(c)) modes, respectively. The platinum atom and oxygen atoms vibrate relatively in x, y and z directions in $E_{u,1}$ (Fig. 3(d)), $E_{u,2}$ (Fig. 3(e)) and A_{2u} (Fig. 3(f)) modes, respectively.

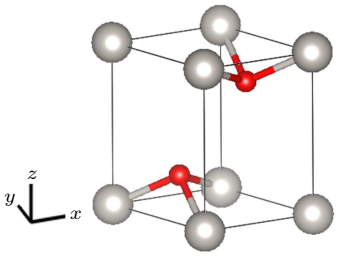


Fig. 1. The crystal structure of α-PtO_2. The gray (red) balls refer to platinum (oxygen) atoms. The solid lines indicate a unit cell. The x, y and z axes are along $[10\bar{1}0]$, $[1\bar{2}10]$ and [0001] directions, respectively.

The α-PtO_2 belongs to D_{3d} point group and $P\bar{3}m1$ space group. According to group theory, the Raman-active modes of α-PtO_2 are A_{1g} and E_g. The vibrational frequency is 15.14 THz for mode A_{1g} and 15.92 THz for mode E_g (double degenerate), which means that we can observe two peaks at 505 cm^{-1} and 531 cm^{-1} in the Raman spectra of α-PtO_2. This is close to the experimental results of 514 cm^{-1} and 560 cm^{-1}.[20]

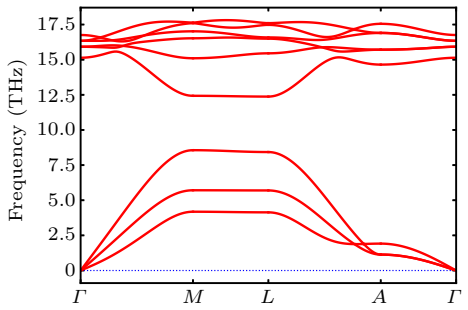


Fig. 2. Phonon dispersion of α-PtO_2.

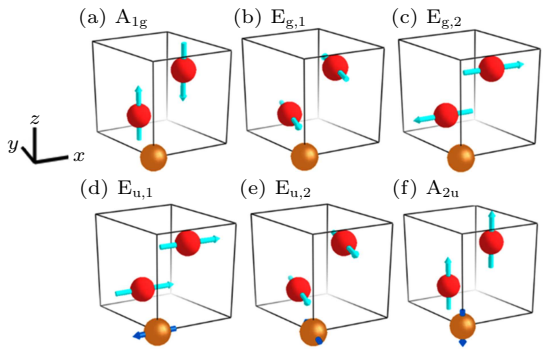


Fig. 3. Atomic movement of the six optical modes at the Γ point.

We also obtain the eigenvectors of A_{1g} mode and E_g modes at the Γ point. Then we calculate the dielectric function variation. The Raman tensor in agreement with the group theory is obtained as follows:

$$R(\mathrm{A_{1g}}) \propto \begin{bmatrix} a & 0 & 0 \\ 0 & a & 0 \\ 0 & 0 & b \end{bmatrix} = \begin{bmatrix} |a|\,\mathrm{e}^{\mathrm{i}\varphi_a} & 0 & 0 \\ 0 & |a|\,\mathrm{e}^{\mathrm{i}\varphi_a} & 0 \\ 0 & 0 & |b|\,\mathrm{e}^{\mathrm{i}\varphi_b} \end{bmatrix},$$

$$R(\mathrm{E_{g,1}}) \propto \begin{bmatrix} c & 0 & 0 \\ 0 & -c & d \\ 0 & d & 0 \end{bmatrix} = \begin{bmatrix} |c|\,\mathrm{e}^{\mathrm{i}\varphi_c} & 0 & 0 \\ 0 & -|c|\,\mathrm{e}^{\mathrm{i}\varphi_c} & |d|\,\mathrm{e}^{\mathrm{i}\varphi_d} \\ 0 & |d|\,\mathrm{e}^{\mathrm{i}\varphi_d} & 0 \end{bmatrix},$$

$$R(\mathrm{E_{g,2}}) \propto \begin{bmatrix} 0 & c & d \\ c & 0 & 0 \\ d & 0 & 0 \end{bmatrix} = \begin{bmatrix} 0 & |c|\,\mathrm{e}^{\mathrm{i}\varphi_c} & |d|\,\mathrm{e}^{\mathrm{i}\varphi_d} \\ |c|\,\mathrm{e}^{\mathrm{i}\varphi_c} & 0 & 0 \\ |d|\,\mathrm{e}^{\mathrm{i}\varphi_d} & 0 & 0 \end{bmatrix}.$$

Table 1. Raman tensor elements.

$\lvert a\rvert$	$\lvert b\rvert$	$\lvert c\rvert$	$\lvert d\rvert$	ψ_a	ψ_b	ψ_c	ψ_d
0.12	0.21	0.30	0.56	−0.66	−1.70	−2.62	1.27

We consider the incident light with wavelengths 633 nm which is commonly used in experiments. The Raman tensor elements are listed in Table 1. Based on the calculated Raman tensor, we compute the Raman scattering intensities by $I\propto\omega_s^4\left|\boldsymbol{e}_s\cdot\boldsymbol{R}\cdot\boldsymbol{e}_i\right|^2$ in parallel polarization configuration and perpendicular polarization configuration. When the wave vector of the incident light is along x direction ($[10\bar{1}]$ direction), its polarization direction can be written as $(0,\cos\theta,\sin\theta)$. In parallel polarization configuration, the polarization direction of the scattered light is parallel to that of the incident light [i.e.

$(0, \cos\theta, \sin\theta)$], while in perpendicular polarization configuration, it is perpendicular to that of the incident light [i.e. $(0, -\sin\theta, \cos\theta)$]. Therefore,

$$I^{\parallel}(\mathrm{A_{1g}}) \propto |a|^2\cos^4\theta + |b|^2\sin^4\theta + \frac{1}{2}\mathrm{Re}(a\cdot b^*)\sin^2(2\theta), \quad (1)$$

$$I^{\parallel}(\mathrm{E_g}) \propto |c|^2\cos^4\theta + |d|^2\sin^2(2\theta) - 2\mathrm{Re}(c\cdot d^*)\cos^2\theta\sin(2\theta), \quad (2)$$

$$I^{\perp}(\mathrm{A_{1g}}) \propto \frac{1}{4}\left[|a|^2+|b|^2-2\mathrm{Re}(a\cdot b^*)\right]\sin^2(2\theta), \quad (3)$$

$$I^{\perp}(\mathrm{E_g}) \propto \frac{1}{4}|c|^2\sin^2(2\theta)+|d|^2\cos^2(2\theta) + \frac{1}{2}\mathrm{Re}(c\cdot d^*)\sin(4\theta). \quad (4)$$

The polar plot of $I^{\parallel}(\mathrm{A_{1g}})$ has two maxima at 90° and 270° (Fig. 4(a)), because $|b| > |a|$, and the second term in Eq. (1) is dominant. The reason for $|b| > |a|$ is that the vibration of atoms is along z direction in $\mathrm{A_{1g}}$ mode (Fig. 3(a)). The two-fold symmetry of the polar plot of $I^{\parallel}(\mathrm{A_{1g}})$ is useful in identifying the orientation of the crystal. The polar plot of $I^{\parallel}(\mathrm{E_g})$ has two maxima near 45° and 135° (Fig. 4(d)), because $|d| > |c|$, and the second term in Eq. (2) is dominant. The polar plot of $I^{\perp}(\mathrm{A_{1g}})$ (Fig. 5(a)) has four maxima at $45°+n\times90°$ ($n=0$, 1, 2, 3) due to the factor $\sin^2(2\theta)$ in Eq. (3). The polar plot of $I^{\perp}(\mathrm{E_g})$ has four maxima near $80°+n\times90°$ ($n=0$, 1, 2, 3) (Fig. 5(d)), because $|d| > |c|$, and the second term in Eq. (4) is dominant.

When the wave vector of the incident light is along y direction ([$1\bar{2}10$] direction), the polarization direction of the incident light can be written as $(\sin\theta, 0, \cos\theta)$. The polarization directions of the scattered light in parallel configuration and perpendicular configuration are $(\sin\theta, 0, \cos\theta)$ and $(\cos\theta, 0, -\sin\theta)$, respectively. Therefore,

$$I^{\parallel}(\mathrm{A_{1g}}) \propto |a|^2\sin^4\theta + |b|^2\cos^4\theta + \frac{1}{2}\mathrm{Re}(a\cdot b^*)\sin^2(2\theta), \quad (5)$$

$$I^{\parallel}(\mathrm{E_g}) \propto |c|^2\sin^4\theta + |d|^2\sin^2(2\theta), \quad (6)$$

$$I^{\perp}(\mathrm{A_{1g}}) \propto \frac{1}{4}\left[|a|^2+|b|^2-2\mathrm{Re}(a\cdot b^*)\right]\sin^2(2\theta), \quad (7)$$

$$I^{\perp}(\mathrm{E_g}) \propto \frac{1}{4}|c|^2\sin^2(2\theta)+|d|^2\cos^2(2\theta). \quad (8)$$

The polar plot of $I^{\parallel}(\mathrm{A_{1g}})$ has two maxima at 0° and 180° (Fig. 4(d)), because $|b| > |a|$, and the second term in Eq. (5) is dominant. The two-fold symmetry of the polar plot of $I^{\parallel}(\mathrm{A_{1g}})$ is useful in identifying the orientation of the crystal. The polar plot of $I^{\parallel}(\mathrm{E_g})$ has four maxima at $45°+n\times90°$ ($n=0$, 1, 2, 3) (Fig. 4(e)), because $|d| > |c|$, and the second term in Eq. (6) is dominant. The polar plot of $I^{\perp}(\mathrm{A_{1g}})$ has four maxima at $45°+n\times90°$ ($n=0$, 1, 2, 3) (Fig. 5(b)) due to the factor $\sin^2(2\theta)$ in Eq. (7). The polar plot of $I^{\perp}(\mathrm{E_g})$ has four maxima near $n\times90°$ ($n=0$, 1, 2, 3) (Fig. 5(e)), because $|d| > |c|$, and the second term in Eq. (8) is dominant.

When the wave vector of the incident light is along z direction ([0001] direction), the polarization direction of the incident light can be written as $(\cos\theta, \sin\theta, 0)$. The polarization directions of the scattered light in parallel configuration and perpendicular configuration are $(\cos\theta, \sin\theta, 0)$ and $(-\sin\theta, \cos\theta, 0)$, respectively. Therefore,

$$I^{\parallel}(\mathrm{A_{1g}}) \propto |a|^2, \quad I^{\parallel}(\mathrm{E_g}) \propto |c|^2,$$
$$I^{\perp}(\mathrm{A_{1g}}) = 0, \quad I^{\perp}(\mathrm{E_g}) \propto |c|^2.$$

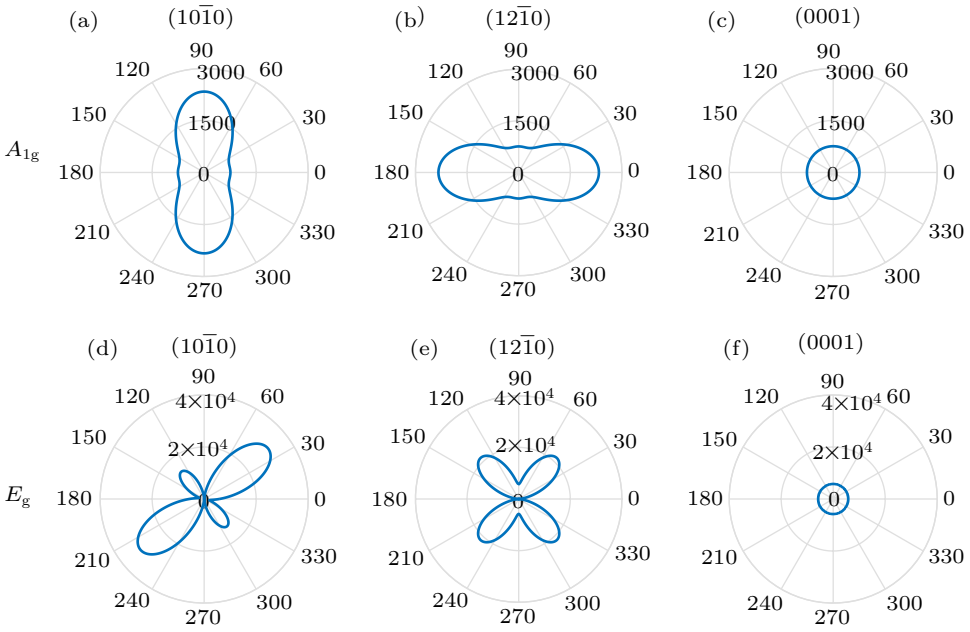


Fig. 4. The polarization-resolved Raman intensities of $\mathrm{A_{1g}}$ mode (top panels) and $\mathrm{E_g}$ (bottom panels) in parallel polarization configuration. The incident light wave vector is along [10$\bar{1}$0] (left panels), [1$\bar{2}$10] (middle panels) and [0001] (right panels) crystal direction, respectively.

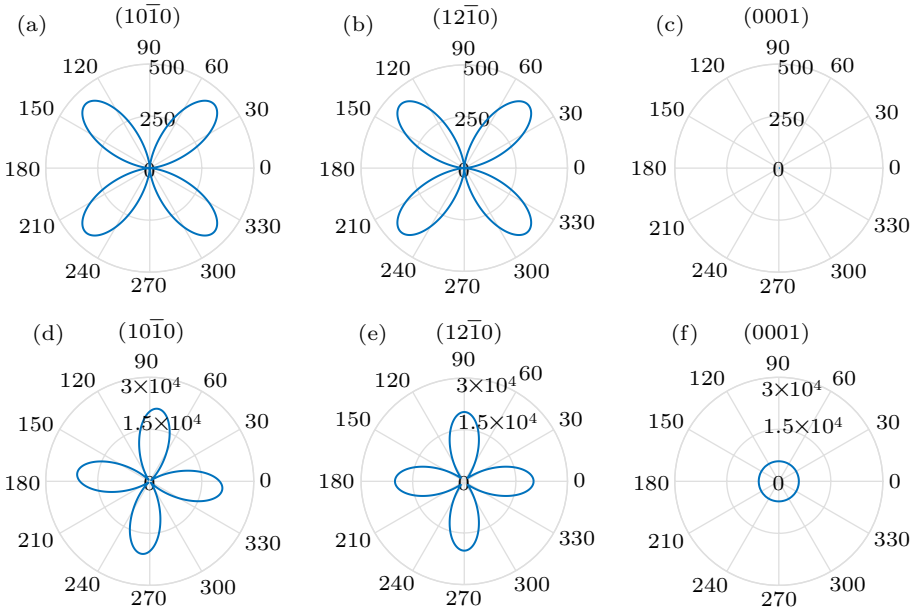


Fig. 5. The polarization-resolved Raman intensities of A_{1g} mode (top panels) and E_g (bottom panels) in perpendicular polarization configuration. The incident light wave vector is along [10$\bar{1}$0] (left panels), [1$\bar{2}$10] (middle panels) and [0001] (right panels) crystal direction, respectively.

The Raman intensity does not depend on θ when the wave vector of the incident light is in z direction.

Comparing the magnitudes of the polar plots, the Raman intensity of the E_g mode is about five times stronger than that of the A_{1g} mode, due to larger value of elements in Raman tensor. The Raman intensity is about three times stronger when the wave vector of the incident light is in x or y direction than in z direction because $|b| > |a|$ and $|d| > |c|$.

4. Conclusion

We have investigated the vibrational properties of α-PtO_2 and calculated the Raman tensor of two Raman-active modes A_{1g} and E_g. The polarization-resolved Raman intensities in parallel polarization configuration and perpendicular polarization configuration are obtained for the cases that the wave vector of incident light is in x, y and z directions. The polar plot of A_{1g} mode in parallel polarization configuration is found to be useful in identifying the orientation of the crystal. The Raman intensity of the E_g mode is about five times stronger than that of the A_{1g} mode. The Raman intensity is about three times stronger when the wave vector of the incident light is in x or y direction than in z direction. Our work will help material scientists to characterize α-PtO_2 and identify its orientation by comparing the experimental spectra with our result.

References

[1] Carothers W H and Adams R 1923 *J. Am. Chem. Soc.* **45** 1071
[2] Voorhees V and Adams R 1922 *J. Am. Chem. Soc.* **44** 1397
[3] Zakharchenko N I 2001 *Russian J. Appl. Chem.* **74** 1686
[4] Gong X Q, Raval R and Hu P 2004 *Phys. Rev. Lett.* **93** 106104
[5] Sabourault N *et al.* 2002 *Org. Lett.* **4** 2117
[6] Jin Z S *et al.* 2003 *J. Mol. Catal a-Chem* **191** 61
[7] Bingwa N A *et al.* 2020 *Molecular Catalysis* **492** 110978
[8] Diniz F B and Ueta R R 2004 *Electrochim. Acta* **49** 4281
[9] Jerkiewicz G *et al.* 2004 *Electrochim. Acta* **49** 1451
[10] Kaewmaraya T *et al.* 2013 *Comput. Mater. Sci.* **79** 804
[11] Blackstock J J, Stewart D R and Li Z 2005 *Appl. Phys. A: Materials Science & Processing* **80** 1343
[12] Chen Q, Li W and Yang Y 2019 *Front. Phys.* **14** 53604
[13] Seriani N *et al.* 2007 *Phys. Rev. B* **76** 155421
[14] Pedersen T M, Li W X and Hammer B 2006 *Phys. Chem. Chem. Phys.* **8** 1566
[15] Gao M R *et al.* 2012 *Chemistry-A European Journal* **18** 8423
[16] H. Neff S H, Hartmannsgruber E, Steinbeiss E, Michalke W, Steenbeck K and Schmidt H G 1996 *J. Appl. Phys.* **79** 7672
[17] Li W X *et al.* 2004 *Phys. Rev. Lett.* **93** 146104
[18] Ouyang G, Sun Q and Zhu W G 2008 *J. Phys. Chem. B* **112** 5027
[19] Yuan J Z M, Yu W *et al* 2015 *Materials* **8** 5007
[20] McBride J R 1991 *J. Appl. Phys.* **69** 1596
[21] Kresse G and Furthmuller J 1996 *Phys. Rev. B* **54** 11169
[22] Perdew J P *et al.* 1992 *Phys. Rev. B* **46** 6671
[23] Adllan A A and Dal Corso A 2011 *J. Phys.: Condens. Matter* **23** 425501
[24] Togo A and Tanaka I 2015 *Scripta Mater.* **108** 1
[25] Massote D V P *et al.* 2016 *Phys. Rev. B* **94** 195416
[26] Ceriotti M, Pietrucci F and Bernasconi M 2006 *Phys. Rev. B* **73** 104304
[27] Deng Z X *et al.* 2019 *Phys. Chem. Chem. Phys.* **21** 1059
[28] Shegai T O and Haran G 2006 *J. Phys. Chem. B* **110** 2459
[29] Kranert C *et al.* 2016 *Sci. Rep.* **6** 165208
[30] Zheng W *et al.* 2015 *Photon. Res.* **3** 38
[31] Luo G F *et al.* 2011 *J. Phys. Chem. C* **115** 24463
[32] Liang L B and Meunier V 2014 *Nanoscale* **6** 5394
[33] Umari P, Pasquarello A and Dal Corso A 2001 *Phys. Rev. B* **63** 094305
[34] Saboori S *et al.* 2019 *ACS Omega* **4** 10171
[35] Jin M G *et al.* 2019 *J. Phys. Chem. C* **123** 29337
[36] Zhu Y M *et al.* 2020 *J. Raman Spectrosc.* **51** 1324
[37] Saboori S *et al.* 2020 *Nanotechnology* **31** 405708
[38] Jin M G *et al.* 2020 *J. Phys. Chem. Lett.* **11** 4311